Dynamic Shaping of Grid Response of Multi-Machine Multi-Inverter Systems Through Grid-Forming IBRs

Preprint

Bala Kameshwar Poolla,[1] Yashen Lin,[1] Andrey Bernstein,[1] Enrique Mallada,[2] and Dominic Groß[3]

1 National Renewable Energy Laboratory
2 Johns Hopkins University
3 University of Wisconsin, Madison

NREL is a national laboratory of the U.S. Department of Energy
Office of Energy Efficiency & Renewable Energy
Operated by the Alliance for Sustainable Energy, LLC

This report is available at no cost from the National Renewable Energy Laboratory (NREL) at www.nrel.gov/publications.

Contract No. DE-AC36-08GO28308

Conference Paper
NREL/CP-5D00-88101
July 2024

Dynamic Shaping of Grid Response of Multi-Machine Multi-Inverter Systems Through Grid-Forming IBRs

Preprint

Bala Kameshwar Poolla,[1] Yashen Lin,[1] Andrey Bernstein,[1] Enrique Mallada,[2] and Dominic Groß[3]

1 National Renewable Energy Laboratory
2 Johns Hopkins University
3 University of Wisconsin, Madison

NOTICE

Dynamic Shaping of Grid Response of Multi-Machine Multi-Inverter Systems Through Grid-Forming IBRs

Bala Kameshwar Poolla, Yashen Lin, Andrey Bernstein
National Renewable Energy Laboratory (NREL)
Golden CO, USA
{bpoolla, yashen.lin, andrey.bernstein}@nrel.gov

Enrique Mallada
Johns Hopkins University
Baltimore MA, USA
mallada@jhu.edu

Dominic Groß
University of Wisconsin
Madison WI, USA
dominic.gross@wisc.edu

Abstract—We consider the problem of controlling the frequency response of weakly-coupled multi-machine multi-inverter low-inertia power systems via grid-forming inverter-based resources (IBRs). In contrast to existing methods, our approach relies on dividing the larger system into multiple strongly-coupled subsystems, without ignoring either the underlying network or approximating the subsystem response as an aggregate harmonic mean model. Rather, through a structured clustering and recursive dynamic shaping approach, the frequency response of the overall system to load perturbations is shaped appropriately. We demonstrate the proposed approach for a three-node triangular configuration and a small-scale radial network. Furthermore, previous synchronization analysis for heterogeneous systems requires the machines to satisfy certain proportionality property. In our approach, the effective transfer functions for each cluster can be tuned by the IBRs to satisfy such property, enabling us to apply the shaping control to systems with a wider range of heterogeneous machines.

Index Terms—inverter-based resources, grid-forming devices, frequency-shaping control, weakly-coupled networks

I. INTRODUCTION

The increasing shift towards decarbonizing the existing grid architecture by integrating renewable energy resources has gathered momentum over the past decade. A large portion of these zero-carbon sources are interfaced to the grid through power electronic devices, commonly known as inverter-based resources (IBRs). These IBRs have very different characteristics from the conventional generators, which could lead to poor system response and even compromise grid stability and resilience in the event of disturbances, as witnessed through several incidents across the globe in recent times [1], [2]. Thus, designing proper control for IBRs is important for maintaining reliable and efficient operation of IBR-integrated grids [3].

The common control strategies include grid-following control, droop-control, and virtual synchronous machines [4]. These strategies usually aim to make the IBRs mimic the

response of synchronous generators, due to the extensive understanding of their operation and control schemes. However, such strategies do not fully exploit the inherent advantages that IBRs have to offer. One alternative is the so-called grid-shaping control, which aims to shape the frequency response of the system to load changes by leveraging the flexible power output of the IBRs [5], [6], [7]. However, these existing shaping controls have limitations: in [5], the approach is designed for grid-following inverters; in [6], the design requires the IBRs to be coherent with the synchronous generator bus, which limits it to systems with strong connectivity. In [7], the grid-shaping control is extended to overcome the strong connectivity assumption.

In this paper, we extend the grid-shaping control in [7] to multi-unit scenarios. In [7], only a single IBR connected to a single machine representing an equivalent grid was considered. In contrast, here, the contribution is the clustering method that allows us to apply the methods from [7] to multi-IBR/multi-machine systems in a systematic way, i.e., dividing the system into smaller subsystems and applying the grid-shaping control design from [7] sequentially. Moreover, in contrast to [6], this work considers network impedances and is not limited to strongly coupled systems. This multi-unit grid-shaping control also relaxes the homogeneity assumptions for turbine time constants in [8], and widens the scope of synchronization results developed therein. We then demonstrate the proposed approach in two use cases. First, for a three-node triangular configuration, the desired target response of the overall system to load perturbations is achieved via a three-step approach involving IBR controller design and kron-reduction. Second, we demonstrate how the grid-shaping approach can be applied to radial small-scale microgrids, through clustering.

II. SYSTEM MODELING

In this work, we investigate shaping the dynamic response of the frequency of a low-inertia power system through grid-forming IBRs. We motivate this by considering a two-node system (see Fig. 1) containing a synchronous machine (SM) that models the aggregate frequency dynamics of a conven-

tional multi-machine power system [8] and a grid-forming voltage source inverter (VSI).

The aggregate response of the SM frequency deviation ω_{sm} to the deviation of the power $p_{\mathrm{sm}} \in \mathbb{R}$ injected by the SM, is modeled by swing dynamics $G_{\mathrm{sw}}(s)$ with a first-order turbine/governor model $G_{\mathrm{tg}}(s)$, where

$$G_{\mathrm{sw}}(s) := \frac{1}{2Hs + \alpha_\ell}, \ G_{\mathrm{tg}}(s) := -\frac{\alpha_{\mathrm{g}}}{\tau s + 1},$$

and results in [8]

$$\omega_{\mathrm{sm}}(s) = -\underbrace{\frac{G_{\mathrm{sw}}(s)}{1 + G_{\mathrm{sw}}(s)G_{\mathrm{tg}}(s)}}_{=:G_{\omega_{\mathrm{sm}}, \, p_{\mathrm{sm}}}(s)} p_{\mathrm{sm}}, \quad (1)$$

where $\alpha_{\mathrm{g}} \in \mathbb{R}_{>0}$ denotes the aggregate speed governor gain (i.e., inverse frequency droop constant), $\alpha_\ell \in \mathbb{R}_{>0}$ denotes the aggregate frequency sensitivity of load, and $\tau \in \mathbb{R}_{>0}$ is the aggregate turbine time constant.
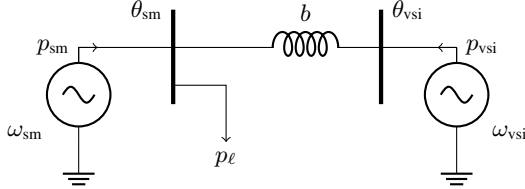

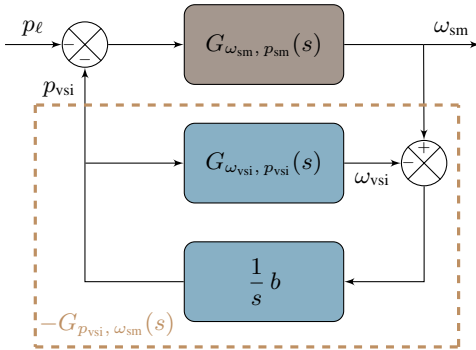Fig. 1: Interconnection of a synchronous machine and grid-forming VSI.

Fig. 2: The synchronous machine–IBR viewed as a feedback system.

Next, consider a VSI coupled to the aggregate frequency dynamics (1) through a lossless transmission line with susceptance $b \in \mathbb{R}_{>0}$ as depicted in Fig. 1. We will refer to the grid as weakly-coupled if b is small (e.g., for grids with low short-circuit ratio) and strongly-coupled if b is large. Notably, this relaxes the assumption in [6] that $b \to \infty$. Next, let $\theta_{\mathrm{vsi}}(s) = \frac{1}{s}\omega_{\mathrm{vsi}}(s)$ and $\theta_{\mathrm{sm}}(s) = \frac{1}{s}\omega_{\mathrm{sm}}(s)$ denote the voltage phase angles at the IBR and SM bus. Then, using the DC power flow approximation at 1 p.u. voltage magnitude and zero angle difference [8], the IBR power injection $p_{\mathrm{vsi}}(s)$ is equal to the power flowing across the line, i.e.,

$$p_{\mathrm{vsi}}(s) = b\left(\theta_{\mathrm{vsi}}(s) - \theta_{\mathrm{sm}}(s)\right) = \frac{1}{s} b\left(\omega_{\mathrm{vsi}}(s) - \omega_{\mathrm{sm}}(s)\right). \quad (2)$$

The combination of the synchronous machine and the IBR can be interpreted as the VSI in feedback with the synchronous machine as shown in Fig. 2. To this end, let

$$\omega_{\mathrm{vsi}}(s) = -G_{\omega_{\mathrm{vsi}}, \, p_{\mathrm{vsi}}}(s) \, p_{\mathrm{vsi}}(s), \quad (3)$$

represent the dynamics of the grid-forming VSI. Combing (2) and (3), the relation between the generator frequency ω_{sm} and the inverter power $p_{\mathrm{vsi}}(s)$ is

$$p_{\mathrm{vsi}}(s) = -\underbrace{\frac{1}{\frac{1}{b}s + G_{\omega_{\mathrm{vsi}}, \, p_{\mathrm{vsi}}}(s)}}_{:= G_{p_{\mathrm{vsi}}, \, \omega_{\mathrm{sm}}}(s)} \omega_{\mathrm{sm}}(s). \quad (4)$$

Using the load perturbation p_ℓ, $p_{\mathrm{sm}} = p_\ell - p_{\mathrm{vsi}}$, and (4) to close the loop between (3) and (1), results in the *closed-loop* transfer function

$$\omega_{\mathrm{sm}}(s) = -\underbrace{\frac{\left(\frac{1}{b}s + G_{\omega_{\mathrm{vsi}}, \, p_{\mathrm{vsi}}}(s)\right) G_{\omega_{\mathrm{sm}}, \, p_{\mathrm{sm}}}(s)}{\frac{1}{b}s + G_{\omega_{\mathrm{sm}}, \, p_{\mathrm{sm}}}(s) + G_{\omega_{\mathrm{vsi}}, \, p_{\mathrm{vsi}}}(s)}}_{:= G^{\mathrm{cl}}_{\omega_{\mathrm{sm}}, \, p_\ell}(s)} p_\ell(s), \quad (5)$$

from the load perturbation p_ℓ to the aggregate frequency ω_{sm}.

In [7], we illustrated that shaping the system response to be *second-order* target transfer functions $G^{\mathrm{cl}\star}_{\omega_{\mathrm{sm}}, \, p_\ell}(s)$ improves the peak power injections from the VSI relative to the approach in [6]. To this end, consider the standalone synchronous machine transfer function $G_{\omega_{\mathrm{sm}}, \, p_{\mathrm{sm}}}(s)$ defined in (1). Let

$$\mathcal{U} := \left\{ \rho \in \mathbb{R} \, \middle| \, 0 \leq \rho < \tau \right\} \quad (6)$$

define the set of effective turbine time constants. Next, consider a candidate transfer function in the form of (1) with an effective turbine time constant $\rho \in \mathcal{U}$, i.e.,

$$G^{\mathrm{cl}\star}_{\omega_{\mathrm{sm}}, \, p_\ell}(s) := -\frac{s\,\rho + 1}{2H\rho\, s^2 + (\alpha_\ell\rho + 2H)\, s + (\alpha_\ell + \alpha_g)}. \quad (7)$$

We wish to design the control transfer function $G_{\omega_{\mathrm{vsi}}, \, p_{\mathrm{vsi}}}(s)$ in order to realize the target function $G^{\mathrm{cl}\star}_{\omega_{\mathrm{sm}}, \, p_\ell}(s)$ for the overall system. Thus, the design problem for the grid-forming VSI transfer function is such that

$$G^{-1}_{p_{\mathrm{vsi}}, \, \omega_{\mathrm{sm}}}(s) = \frac{1}{b}\, s + G_{\omega_{\mathrm{vsi}}, \, p_{\mathrm{vsi}}}(s) \overset{!}{=} \frac{(s\,\tau + 1)(s\,\rho + 1)}{\alpha_g\, s\,(\tau - \rho)}. \quad (8)$$

We note that the right hand side terms of (8) can be realized through a Proportional-Integral-Derivative (PID) type controller $G_{\omega_{\mathrm{vsi}}, \, p_{\mathrm{vsi}}}(s)$, i.e.,

$$G_{\omega_{\mathrm{vsi}}, \, p_{\mathrm{vsi}}}(s) = k_p + \frac{k_i}{s} + k_d\, s, \quad (9)$$

with the PID control gains

$$k_d := \frac{\tau\,\rho}{\alpha_g(\tau - \rho)} - \frac{1}{\hat{b}}, \ k_p := \frac{\tau + \rho}{\alpha_g(\tau - \rho)}, \ k_i := \frac{1}{\alpha_g(\tau - \rho)}, \quad (10)$$

where $\hat{b}$ is an exact estimate for b.

2

III. Multi-IBR Three-Node Triangular Systems

In the previous section, we considered systems with one VSI. When appropriately chosen, the controller gains result in an overall second-order, closed-loop response while also minimizing peak power injections. The understanding developed for the two-node scenario enables us to design controller gains in systems with more than one VSI, by sequentially applying the approach. To illustrate this we start with a three-node triangular configuration with two VSIs.

Consider a three-node system comprising one aggregate machine model and two IBRs connected in a triangular configuration, through lossless transmission lines with susceptances b_{12}, b_{1s}, $b_{2s} \in \mathbb{R}_{>0}$ as depicted in Fig. 3. Let the Laplacian matrix of this network be L. Consider a load perturbation $p_\ell(s)$ at the machine bus. Let $p_{\text{vsi},1}(s)$, $p_{\text{vsi},2}(s)$, and $p_{\text{sm}}(s)$ be the resulting power injections from the VSIs and the machine; $p_{12}(s)$, $p_{1s}(s)$, and $p_{2s}(s)$ be the power flows on the lines; $\theta_{\text{vsi},1}(s)$, $\theta_{\text{vsi},2}(s)$, and $\theta_{\text{sm}}(s)$ denote the voltage angles at the buses. Then, under DC power flow approximations at 1 p.u. voltage magnitude and zero angle difference, we have $p_{12}(s) = b_{12}(\theta_{\text{vsi},1}(s) - \theta_{\text{vsi},2}(s))$, $p_{1s}(s) = b_{1s}(\theta_{\text{vsi},1}(s) - \theta_{\text{sm}}(s))$, and $p_{2s}(s) = b_{2s}(\theta_{\text{vsi},2}(s) - \theta_{\text{sm}}(s))$. Finally, let the dynamics of the VSIs and the aggregate generator be captured through the transfer functions $G_{\text{vsi},1}(s)$, $G_{\text{vsi},2}(s)$, and $G_{\text{sm}}(s)$ respectively. The relationships between the power injections and the frequency excursions at the buses are

$$\omega_1(s) = -G_{\text{vsi},1}(s)\, p_{\text{vsi},1}(s),\ \omega_2(s) = -G_{\text{vsi},2}(s)\, p_{\text{vsi},2}(s)$$
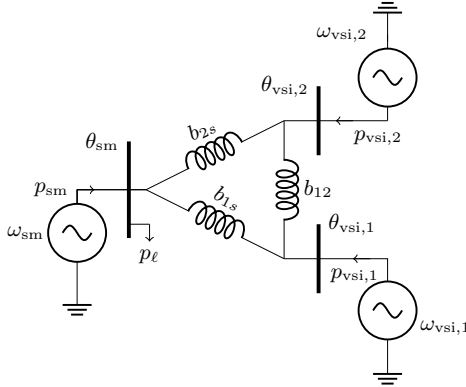$$\omega_{\text{sm}}(s) = -G_{\text{sm}}(s)\, p_{\text{sm}}(s). \tag{11}$$

Fig. 3: Three-node triangular configuration with two IBRs.

Designing the transfer functions $G_{\text{vsi},1}(s)$, $G_{\text{vsi},2}(s)$ for the VSIs, such that the resulting frequency dynamics depict certain characteristic behaviors is complex. Previous solutions assume strong coupling and approximate the overall response as a harmonic mean of the individual transfer functions [9]. An alternative approach, without these assumptions, is the sequential application of the shaping algorithm, in which the gains are functions of the network coupling. To this end, we propose a three-step approach as illustrated in Fig. 4.

(i) In the first step, we choose one VSI device ($G_{\text{vsi},1}(s)$), and the synchronous machine $G_{\text{sm}}(s)$ (with an original turbine time constant τ) as a two-node subsystem, without considering their connection with the other node.

(ii) Next, we *(a)* shape the frequency response of this two-node subsystem, i.e., determine the control gains for the VSI device in step 1 ($G_{\text{vsi},1}(s)$), such that closed-loop (with the VSI) transfer function from the load perturbation to the frequency of the machine is equivalent to the dynamics of a machine with a time constant ρ (c.f. Section II); *(b)* compute the kron-reduced admittance between (SG+VSI$_1$) and VSI$_2$ after eliminating the node with VSI$_1$. This gives us a new equivalent two-node system, as shown in Fig. 4.

(iii) Finally, we determine the gains of the other VSI device ($G_{\text{vsi},2}(s)$), such that the closed-loop transfer function (from load perturbation to machine frequency) represents the dynamics of a machine with a time constant ζ and other parameters equal to ones in G_{sm}.
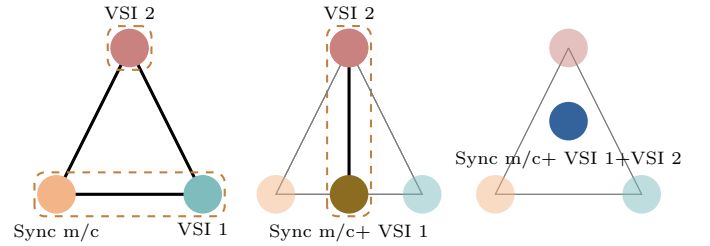

Fig. 4: Three-step approach for three-node triangular networks.

Mathematically, as the structure of the problem still remains as in the previous section, we can realize the VSI transfer functions through PID type controllers, i.e.,

$$G_{\omega_{\text{vsi}}, m}(s) = k_{p,m} + \frac{k_{i,m}}{s} + k_{d,m}\, s,\ \forall m \in \{1, 2\}$$

with the PID control gains

$$k_{d,1} := \frac{\tau\,\rho}{\alpha_g(\tau - \rho)} - \frac{1}{b_{1s}},\ k_{p,1} := \frac{\tau + \rho}{\alpha_g(\tau - \rho)},\ k_{i,1} := \frac{1}{\alpha_g(\tau - \rho)},$$
$$k_{d,2} := \frac{\zeta\,\rho}{\alpha_g(\rho - \zeta)} - \frac{1}{b_{\text{kron}}},\ k_{p,2} := \frac{\rho + \zeta}{\alpha_g(\rho - \zeta)},\ k_{i,2} := \frac{1}{\alpha_g(\rho - \zeta)},$$

where b_{kron} is the susceptance for the kron-reduced network (removing node 1). While we assume complete knowledge of the network, the gains may also be computed using parameter estimates as in [7]. However, due to space constraints, a stability and robustness analysis when using estimates is deferred to future work.

Next, we present some simulation results for a three-node triangular system with gains determined from the three-step approach discussed above. To this end, consider a network as in Fig. 3, with synchronous machine parameters from [7]. Let $b_{12} = 100$ p.u., $b_{1s} = 200$ p.u., and $b_{2s} = 150$ p.u. Let the desired target response from the overall system be a second-order response with an effective time-constant of 0.8s. To this end, we first design the gains of VSI$_1$, such that its combination with the synchronous machine has an effective time constant of $\rho = 0.9$s, with other parameters unchanged. Next, the gains of VSI$_2$ are computed such that the overall system is an equivalent synchronous machine with second-order dynamics and a time constant $\zeta = 0.8$s. Note that, the
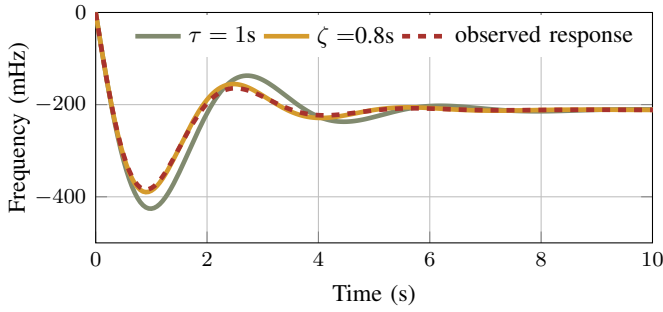
3

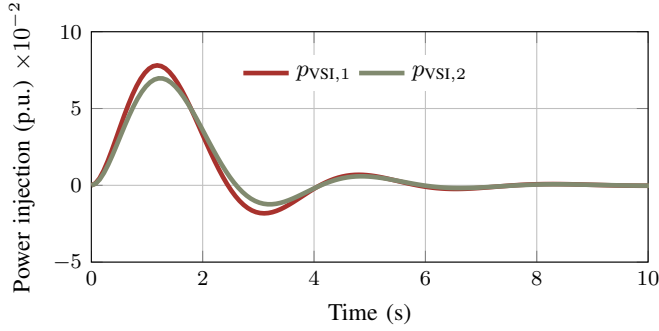Fig. 5: The frequency responses for a 1 p.u. load step.

Fig. 6: The IBR power injections for the two VSIs for a 1 p.u. load step.

grid-shaping approach inherently ensures that the peak IBR power injections are minimized.

In Fig. 5, we illustrate the frequency response of the system to a 1 p.u. load step. The observed response corresponds to computing the frequency dynamics for the three-node triangular network, after substituting the resulting transfer functions for the two VSIs and the synchronous machine. Note that this is almost identical to the desired response, i.e., a synchronous machine with a time constant of $\zeta = 0.8$s. Furthermore, we note the improvement in frequency nadir compared to the original system with $\tau = 1$s. The corresponding power injections from the VSIs are presented in Fig. 6.

IV. SMALL-SCALE RADIAL MICROGRIDS

In this section, we investigate controller design for isolated small-scale radial networks with multiple VSIs and SMs. To this end, we review two concepts: clustering in power grids [10], and proportionally heterogeneous machines [8]. These two ideas along with the sequential application of dynamic frequency shaping become the basis for our design.

A. Background

The motivation for clustering in power systems is to dynamically identify sets of nodes/buses (chosen from the entire network) that are strongly coupled. We recall that for any given network with a laplacian L, the eigenvector $\nu_2(L)$ corresponding to the second smallest eigenvalue $\lambda_2(L)$ (also referred to as the algebraic connectivity) is known as the Fiedler vector. The elements of this vector provide a natural network partition into two components, based on their sign, i.e., $\nu_2(L)_i \leq 0$ or $\nu_2(L)_i > 0$. Specifically, the Fiedler vector-based clustering

is applied recursively, respecting the following assumptions, until no further clusters can be obtained:

 (i) The resulting clusters at each step should only consist of connected components (i.e., partitioning based on the obtained clusters, does not result in disconnected nodes).
 (ii) The final set of clusters should each have only one aggregate synchronous generator. (Note that the aggregate synchronous machine is an equivalent representation of strongly-coupled multiple machines.)

These assumptions though appearing somewhat restrictive, can still be applied to a wide range of networks.

Next, we revisit aggregate modeling of proportionally heterogeneous machines. Most of the control-theoretic analysis in power systems has traditionally relied on the assumption of homogeneity of machines. In order to cover more generic scenarios, the authors in [8] proposed a theory for parameters satisfying a certain proportionality. Specifically, for a *representative machine* transfer function $g_0(s)$ and a *rating parameter* f_i, the transfer function for a generator at bus i is

$$g_i(s) = \frac{1}{f_i} g_0(s).$$

While such a proportionality assumption f_i can be tied to the rating of the machines and is intuitive for transfer functions of the form $G_{sw}(s)$, it is only justified for second-order transfer functions (1), provided $H_i = f_i H_0$, $\alpha_{g_i} = f_i \alpha_{\ell 0}$, $\alpha_{\ell i} = f_i \alpha_{\ell 0}$, and $\tau_i = \tau$. The turbine time constant is assumed to be homogeneous for all generators regardless of their ratings. In contrast, with the frequency shaping approach from grid-forming IBRs, this assumption is no longer necessary, as the turbine time constants can be made equal for all generators in a network, extending the applicability of synchronization results in [8] to real-world systems.

B. Modified IEEE-13 network case-study

Consider a modified IEEE-13 network as depicted in Fig. 7(a), with one synchronous machine each at nodes 9 and 5. Further, the network comprises two grid-forming IBRs at nodes 11 and 12. Finally, let node 9 be perturbed by a disturbance $p_\ell(s)$.
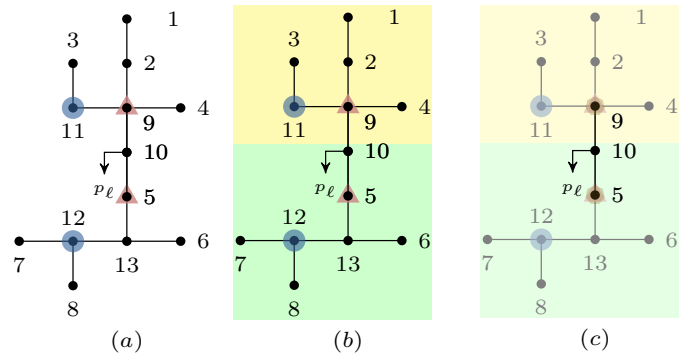

Fig. 7: Grid-shaping approach for radial microgrids.

A classic approach to designing IBR controllers in such a scenario involves matching the harmonic mean of the overall

4

system to a desired transfer function. This approach is reasonable when the network is strongly coupled. However, neglecting the underlying network topology and admittance can be fraught with risks when designing the controls in weakly-coupled grids, and more so in the absence of proper grid parameters [7]. Furthermore, the ability of grid-shaping IBRs to tune the turbine time constants of the coupled synchronous machines makes grid-shaping a more attractive alternative.

To design the IBR controls, we follow the following approach. First, we determine the partitions/clusters using the network Laplacian's Fiedler vector $\nu_2(L)$. For the IEEE-13 network under consideration, this results in two clusters as indicated in Fig. 7(b). Next, in each cluster, we apply Kron reduction techniques [11] removing all nodes without an IBR, a machine, or load perturbation; and then computing the effective susceptance between the IBRs and machines. The IBR controller gains are then selected using the grid-shaping approach[1] such that the turbine time constants of all synchronous machines become identical. This reduces the original network to Fig. 7(c), where nodes 9 and 5 represent the aggregate machine and IBR dynamics. For larger radial networks, this process is continued recursively, until we can have no more partitions.

To validate the approach through simulations, we consider a 1 p.u. load step at bus 10 with the representative synchronous machine parameters for $g_0(s)$ from [7], the rating parameter $f_9 = 1$, $\tau_9 = 1.2$s for the machine at bus 9, $f_5 = 1.5$, $\tau_5 = 1.5$s for the machine at bus 5. The IBRs modify the effective time constant of both the machines to be 1s. In Fig. 8, the frequency excursions before and after the IBR action are illustrated. Note that the frequency nadir for both generators improves after the IBR power injection. Furthermore, as in the original network node, 5 is closer to the disturbance node 10 as compared to 9, we have a larger power injection and a greater frequency change observed at 5. Finally, we plot the weighted COI frequency ($\bar{\omega}_{COI}$), which coincides with the target frequency ($\bar{\omega}_t$), i.e., the theoretic coherent frequency for proportionally heterogeneous machines (cf. (16) in [8]). The corresponding VSI injections are presented in Fig. 9.

V. CONCLUSIONS

We extended the grid-forming frequency shaping control for weakly-coupled grids to multi-unit scenarios. This was achieved by dividing the larger system into smaller subsystems, and iteratively applying the single generator, single IBR controller design solution [7]. Compared to previous works, which considered a harmonic mean approximate solution (i.e., ignores the parameters of the underlying network), our approach resulted in the controller gains being explicit functions of these parameters. The multi-unit shaping control was then validated through simulations on two classes of networks, the three-node triangular configuration, and small-scale radial microgrids. As part of future work, we aim to leverage this structured approach for large-scale, mesh-connected networks.

[1]Note that we can do this as there are only two nodes left in the cluster.
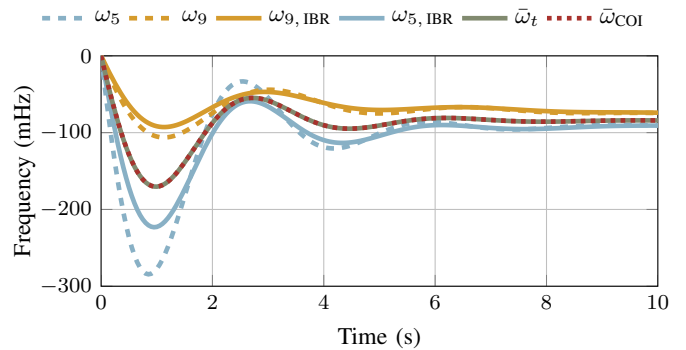

Fig. 8: The frequency responses for a 1 p.u. load step.
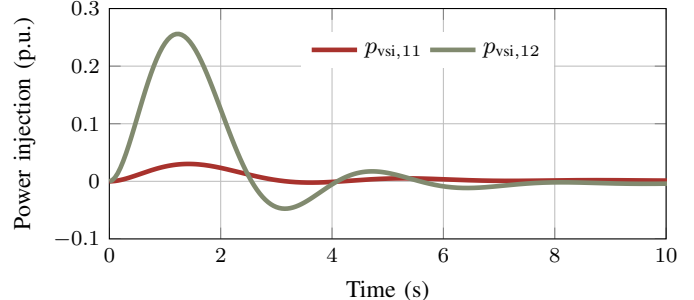

Fig. 9: The IBR power injections at nodes 11, 12 for a 1 p.u. load step.

We will also explore techniques to update control gains when the network structure and number of inverters are varied.

REFERENCES

[1] F. Milano, F. Dörfler, G. Hug, D. J. Hill, and G. Verbič, "Foundations and challenges of low-inertia systems (invited paper)," in *Power Systems Computation Conference*, 2018.

[2] R. W. Kenyon, M. Bossart, M. Marković, K. Doubleday, R. Matsuda-Dunn, S. Mitova, S. A. Julien, E. T. Hale, and B.-M. Hodge, "Stability and control of power systems with high penetrations of inverter-based resources: An accessible review of current knowledge and open questions," *Solar Energy*, vol. 210, pp. 149–168, 2020.

[3] B. Kroposki, B. Johnson, Y. Zhang, V. Gevorgian, P. Denholm, B.-M. Hodge, and B. Hannegan, "Achieving a 100% renewable grid: Operating electric power systems with extremely high levels of variable renewable energy," *IEEE Power and Energy Mag.*, vol. 15, no. 2, pp. 61–73, 2017.

[4] Y. Lin, J. H. Eto, B. B. Johnson, J. D. Flicker, R. H. Lasseter, H. N. Villegas Pico, G.-S. Seo, B. J. Pierre, and A. Ellis, "Research roadmap on grid-forming inverters," NREL, USA, Tech. Rep., 2020.

[5] Y. Jiang, E. Cohn, P. Vorobev, and E. Mallada, "Storage-based frequency shaping control," *IEEE Trans. Power Syst.*, vol. 36, no. 6, pp. 5006–5019, 2021.

[6] Y. Jiang, A. Bernstein, P. Vorobev, and E. Mallada, "Grid-forming frequency shaping control for low-inertia power systems," in *American Control Conference*, 2021, pp. 4184–4189.

[7] B. K. Poolla, Y. Lin, A. Bernstein, E. Mallada, and D. Groß, "Frequency shaping control for weakly-coupled grid-forming IBRs," *IEEE Control Systems Letters*, vol. 7, pp. 937–942, 2022.

[8] F. Paganini and E. Mallada, "Global analysis of synchronization performance for power systems: Bridging the theory-practice gap," *IEEE Transactions on Automatic Control*, vol. 65, no. 7, pp. 3007–3022, 2020.

[9] H. Min, R. Pates, and E. Mallada, "A frequency domain analysis of slow coherency in networked systems," 2023, submitted. [Online]. Available: https://mallada.ece.jhu.edu/pubs/2023-Preprint-MPM.pdf

[10] J. Guo, G. Hug, and O. K. Tonguz, "Intelligent partitioning in distributed optimization of electric power systems," *IEEE Transactions on Smart Grid*, vol. 7, no. 3, pp. 1249–1258, 2016.

[11] F. Dorfler and F. Bullo, "Kron reduction of graphs with applications to electrical networks," *IEEE Transactions on Circuits and Systems I: Regular Papers*, vol. 60, no. 1, pp. 150–163, 2013.

5